Published by :
https://www.ijert.org/
An International Peer-Reviewed Journal

International Journal of Engineering Research & Technology (IJERT)
ISSN: 2278-0181
Vol. 15 Issue 04 , April - 2026

Comparative Performance Analysis of Conventional PI and LMS-Based Adaptive Speed Control for BLDC Motor

Malothu Shilpa, Kadasi Rohan, Korra Akash, Dr. Ch. Vinay Kumar
Department of Electrical and Electronics Engineering
Mahatma Gandhi Institute Of Technology
Hyderabad, India

***Abstract*—Brushless DC (BLDC) motors are extensively utilized in industrial automation, electric vehicles (EVs), aerospace, and household appliances due to their high power density, superior efficiency, fast dynamic response, and extended operational lifespan. Despite these advantages, achieving precise and robust speed control under varying load conditions, magnetic saturation, and parameter uncertainties remains a formidable challenge when employing conventional Proportional-Integral (PI) or Proportional-Integral-Derivative (PID) controllers. This paper presents an exhaustive design, implementation, and comparative performance analysis of a neural-network-based and Least Mean Square (LMS) adaptive speed controller tailored to enhance the dynamic response and stability of a BLDC motor drive system. An Artificial Neural Network (ANN) featuring a feed-forward multi-layer perceptron topology is synthesized and trained to estimate optimal control signals by learning the highly nonlinear dynamics of the motor. Simultaneously, an LMS adaptive controller is integrated to continuously update control weights based on instantaneous speed tracking errors. Extensive time-domain simulations are executed in the MATLAB/Simulink environment. The proposed adaptive control strategies are rigorously evaluated against a finely tuned traditional PI controller under an array of operating scenarios, including sudden load torque variations, reference speed step changes, and steady-state operations. Key performance indicators—such as rise time, settling time, steady-state error, percent overshoot, and electromagnetic torque ripple—are quantified. The empirical results unequivocally demonstrate that the LMS-based and ANN adaptive controllers provide a significantly faster dynamic response, virtual elimination of steady-state error, reduced overshoot, and vastly superior disturbance rejection capabilities compared to conventional linear control methodologies.**

***Index Terms*—Brushless DC (BLDC) Motor, Least Mean Square (LMS) Algorithm, Artificial Neural Networks (ANN), Adaptive Speed Control, Proportional-Integral (PI) Controller, Electric Vehicles, Torque Ripple Reduction.**

I. Introduction

BRUSHLESS Direct Current (BLDC) motors have progressively supplanted conventional brushed DC and induction motors across a spectrum of modern, high-performance applications. Characterized by their electronically commutated stators and permanent magnet rotors, BLDC motors eliminate the mechanical friction, sparking, and wear associated with traditional brush-and-commutator assemblies. This architectural shift yields exceptionally high operational efficiency, a compact form factor, high torque-to-weight ratios, and superior thermal dissipation capabilities. Consequently, BLDC motors have become the propulsion technology of choice for electric vehicles (EVs), unmanned aerial vehicles (drones), precision robotics, and advanced HVAC systems [1].

However, the inherent advantages of BLDC motors are accompanied by complex control requirements. The dynamic behavior of a BLDC motor is highly nonlinear. These nonlinearities manifest through trapezoidal back-electromotive force (back-EMF) profiles, localized magnetic saturation, cogging torque stemming from the interaction between the permanent magnets and stator slots, and position-dependent phase inductances. Traditional linear controllers, particularly the ubiquitous Proportional-Integral (PI) and Proportional-Integral-Derivative (PID) controllers, are typically tuned around a specific nominal operating point. While they provide satisfactory steady-state regulation under these nominal conditions, their performance rapidly degrades when subjected to parameter variations, sudden load disturbances, or operation across a wide speed range.

To mitigate these limitations, advanced control algorithms rooted in artificial intelligence (AI) and machine learning (ML) have garnered significant attention. Neural networks (NNs) and adaptive filtering algorithms, such as the Least Mean Square (LMS) algorithm, possess inherent capabilities for nonlinear function approximation and dynamic adaptation. By continuously learning the evolving dynamic state of the motor, these intelligent controllers can adjust their internal parameters in real-time to maintain optimal performance despite external perturbations or internal parameter shifts.

This paper is structured to provide a comprehensive exploration of adaptive BLDC motor control. Section II details the fundamental construction and operation of BLDC motors. Section III provides an extensive mathematical state-space model of the BLDC drive. Section IV outlines the limitations of conventional PI control. Sections V and VI propose and detail the architecture of the LMS adaptive and Neural Network controllers. Section VII presents the simulation setup, while Section VIII offers a deep comparative analysis of the results. Section IX concludes the research.

International Journal of Engineering Research & Technology (IJERT)
ISSN: 2278-0181
Vol. 15 Issue 04 , April - 2026

II. BLDC Motor Fundamentals and Topology

A. Electromechanical Construction

A standard BLDC motor comprises a stationary stator and a rotating rotor. The stator is constructed from stacked steel laminations featuring slots that house the polyphase windings (typically three-phase). Unlike AC synchronous motors which rely on sinusoidal spatial flux distribution, BLDC stator windings are specifically designed to produce a trapezoidal back-EMF profile.

The rotor utilizes high-energy permanent magnets—commonly Neodymium-Iron-Boron (NdFeB) or Samarium-Cobalt (SmCo)—surface-mounted or embedded within the rotor core. This design eliminates the need for rotor windings and slip rings, drastically reducing rotor inertia and allowing for exceptional dynamic acceleration profiles.

B. Electronic Commutation Principle

Because mechanical commutators are absent, BLDC motors require an external electronic inverter to direct current into the appropriate stator phases synchronously with the rotor's magnetic poles. This process, known as electronic commutation, is governed by the Lorentz force law.

To achieve optimal torque production, the stator flux vector must be maintained orthogonally (at 90 electrical degrees) to the rotor flux vector. This necessitates precise knowledge of the rotor position, typically acquired via three strategically placed Hall-effect sensors mounted on the stator. These sensors detect the magnetic polarity of the passing rotor magnets and generate a three-bit digital sequence that repeats every 360 electrical degrees. A digital decoder translates this sequence into six distinct gating states for the three-phase inverter, ensuring that only two stator phases are energized simultaneously (120-degree conduction mode) while the third remains unenergized to observe back-EMF for sensorless applications.

III. Problem Statement and Control Challenges

The precise regulation of speed and torque in BLDC drives is complicated by a multitude of intersecting physical phenomena:

1) **Nonlinear Back-EMF Distortion:** While theoretically trapezoidal, manufacturing imperfections, winding distributions, and flux fringing cause the back-EMF waveform to deviate from the ideal shape, directly inducing torque pulsations.
2) **Magnetic Saturation:** High transient currents required during rapid acceleration or heavy load conditions can saturate the stator core. This nonlinear flux-current relationship alters the effective inductance and drastically shifts the motor's dynamic response.
3) **Cogging Torque:** The magnetic attraction between the rotor magnets and the stator teeth causes a periodic reluctance torque, noticeable at low speeds, which introduces mechanical vibrations and tracking errors.
4) **Commutation Transients:** The finite di/dt limits imposed by phase inductance mean that phase currents cannot change instantaneously during the electronic switching events. This overlap results in periodic "commutation torque ripple" occurring six times per electrical cycle.

IV. Comprehensive Mathematical Modeling

To design a highly responsive adaptive controller, an accurate mathematical model of the BLDC motor is strictly required. Assuming a symmetrical three-phase star-connected stator, uniform air-gap, and negligible iron losses, the electrical dynamics can be modeled using the following matrix equation:

$$\begin{bmatrix} v_a \\ v_b \\ v_c \end{bmatrix} = \begin{bmatrix} R & 0 & 0 \\ 0 & R & 0 \\ 0 & 0 & R \end{bmatrix} \begin{bmatrix} i_a \\ i_b \\ i_c \end{bmatrix} + \begin{bmatrix} L-M & 0 & 0 \\ 0 & L-M & 0 \\ 0 & 0 & L-M \end{bmatrix} \frac{d}{dt} \begin{bmatrix} i_a \\ i_b \\ i_c \end{bmatrix} + \tag{1}$$

Where:

- v_a, v_b, v_c are the applied stator phase voltages.
- i_a, i_b, i_c are the stator phase currents.
- e_a, e_b, e_c are the trapezoidal back-EMFs.
- R is the stator phase resistance.
- L is the self-inductance of each phase.
- M is the mutual inductance between phases.

Because the neutral point is isolated, $i_a + i_b + i_c = 0$. The back-EMF of each phase is a function of rotor speed (ω) and rotor position (θ):

$$e_x = K_e \cdot f_x(\theta) \cdot \omega \quad \text{for } x \in \{a, b, c\} \tag{2}$$

Where K_e is the back-EMF constant, and $f_x(\theta)$ represents the normalized trapezoidal shape function bounded by $[-1, 1]$.

The total electromagnetic torque (T_e) generated by the interaction of phase currents and back-EMF is derived from the conservation of power:

$$T_e = \frac{e_a i_a + e_b i_b + e_c i_c}{\omega} \tag{3}$$

The mechanical equation of motion, linking torque to angular velocity, is:

$$J\frac{d\omega}{dt} + B\omega = T_e - T_L \tag{4}$$

Where J is the combined rotor and load inertia, B is the viscous friction coefficient, and T_L is the external load torque.

A. Parameter Identification

The specific parameters utilized in this study are detailed in Table I. The electrical time constant ($\tau_e = L/R \approx 0.0425$ s) is significantly faster than the mechanical time constant ($\tau_m = J/B \approx 0.2$ s), ensuring a rapid current loop response.

V. Conventional PI Control Architecture

The conventional approach to BLDC speed regulation involves a cascaded loop structure: an inner current (torque) loop and an outer speed loop. The speed error, $e(t) = \omega_{ref}(t) - \omega_{act}(t)$, is processed by the PI controller to generate the reference torque/current signal.

International Journal of Engineering Research & Technology (IJERT)
ISSN: 2278-0181
Vol. 15 Issue 04 , April - 2026

TABLE I
BLDC MOTOR SYSTEM PARAMETERS

Parameter Name	Symbol	Value
Stator Resistance	R	$0.2\,\Omega$
Stator Inductance	L	8.5 mH
DC Bus Voltage	V_{dc}	311 V
Torque Constant	K_t	0.65 Nm/A
Back-EMF Constant	K_e	0.65 V $\cdot$ s/rad
Rotor Inertia	J	0.0025 kg $\cdot$ m^2
Viscous Friction	B	0.001 Nm $\cdot$ s/rad
Nominal Load Torque	T_L	10 Nm

The continuous-time transfer function of the PI controller is:

$$C(s) = K_p + \frac{K_i}{s} = K_p \left(1 + \frac{1}{T_i s}\right) \tag{5}$$

Using the mathematical parameters from Section IV, the closed-loop characteristic equation under PI control yields roots that dictate the system's settling time. For instance, with $K_p = 3.3$ and an overly large integral time constant ($T_i = 300$ s), the dominant pole approaches the origin ($s \approx -0.003$), resulting in sluggish steady-state error elimination. Re-tuning the integral gain improves response time but often at the cost of excessive overshoot during sudden load application.

VI. Proposed Adaptive Control Methodologies

A. Least Mean Square (LMS) Adaptive Controller

To transcend the limits of fixed-gain PI controllers, an LMS-based adaptive filter is embedded within the control loop. The LMS algorithm is a stochastic gradient descent method that dynamically adapts the controller's coefficients to minimize the mean square of the speed error.

Let the digital error at sampling instant n be:

$$e(n) = \omega_{ref}(n) - \omega_{act}(n) \tag{6}$$

The adaptive control signal $u(n)$ (which determines the PWM duty cycle) is generated by taking the inner product of the weight vector $\mathbf{w}(n)$ and the input signal vector $\mathbf{x}(n)$:

$$u(n) = \mathbf{w}^T(n)\mathbf{x}(n) \tag{7}$$

The weights are updated iteratively using the LMS learning rule:

$$\mathbf{w}(n+1) = \mathbf{w}(n) + \mu \cdot e(n) \cdot \mathbf{x}(n) \tag{8}$$

Where μ is the adaptive learning rate step size. A critical design requirement is bounding μ to ensure algorithmic convergence without inducing instability. The stability criterion mandates that $0 < \mu < \frac{2}{\lambda_{max}}$, where λ_{max} is the largest eigenvalue of the input signal's autocorrelation matrix. By dynamically updating $\mathbf{w}(n)$, the controller seamlessly adapts to variations in J, B, or sudden introductions of T_L.

B. Artificial Neural Network (ANN) Topology

An alternative approach developed in this study utilizes a Multi-Layer Perceptron (MLP) Artificial Neural Network. The ANN acts as an intelligent predictive controller capable of highly nonlinear mapping. The network architecture comprises:

- **Input Layer:** Accepts speed error $e(n)$ and change in error $\Delta e(n)$.
- **Hidden Layers:** Two hidden layers employing sigmoidal activation functions ($f(x) = \frac{1}{1+e^{-x}}$) to capture the motor's saturation and ripple dynamics.
- **Output Layer:** A linear activation function generating the optimal reference current command I^*_{ref}.

The network is pre-trained using Levenberg-Marquardt backpropagation on datasets derived from the detailed BLDC mathematical model, ensuring a robust starting point before real-time online adaptation begins.

VII. Simulation and System Design

The complete closed-loop system is modeled in MATLAB/Simulink R2023b using the Simscape Electrical libraries.

A. System Components

- **DC Voltage Source:** Provides a stiff 311 V bus (rectified 220 V AC).
- **Universal Bridge Inverter:** A 6-switch IGBT/Diode inverter operating at a switching frequency of 10 kHz.
- **PWM Generator:** Modulates the duty cycle output from the LMS controller and aligns it with the commutation logic.
- **Decoder:** Converts three-phase trapezoidal back-EMF zero-crossing data into discrete Hall-effect signals for 120-degree commutation.

VIII. Simulation Results and Dynamic Analysis

The system was subjected to rigorous step-response testing, with the reference speed commanded to step from 0 to 500 rad/s under a nominal load torque of 10 Nm.

A. Speed Tracking Performance

Figure 2 illustrates the comparative transient speed response.

Under the fixed PI controller, the system accelerated to a steady-state value of 490.4 rad/s, failing to completely eliminate the error due to parameter mismatches and steady-state load drop. Conversely, the LMS adaptive controller demonstrated aggressive initial learning, rapidly tuning its weights via Equation 8 to push the motor speed to exactly 499.3 rad/s. This equates to a negligible tracking error of $\sim 0.14\%$. Furthermore, the LMS response exhibited a monotonic, critically damped rise characteristic with absolutely zero overshoot.

International Journal of Engineering Research & Technology (IJERT)
ISSN: 2278-0181
Vol. 15 Issue 04 , April - 2026

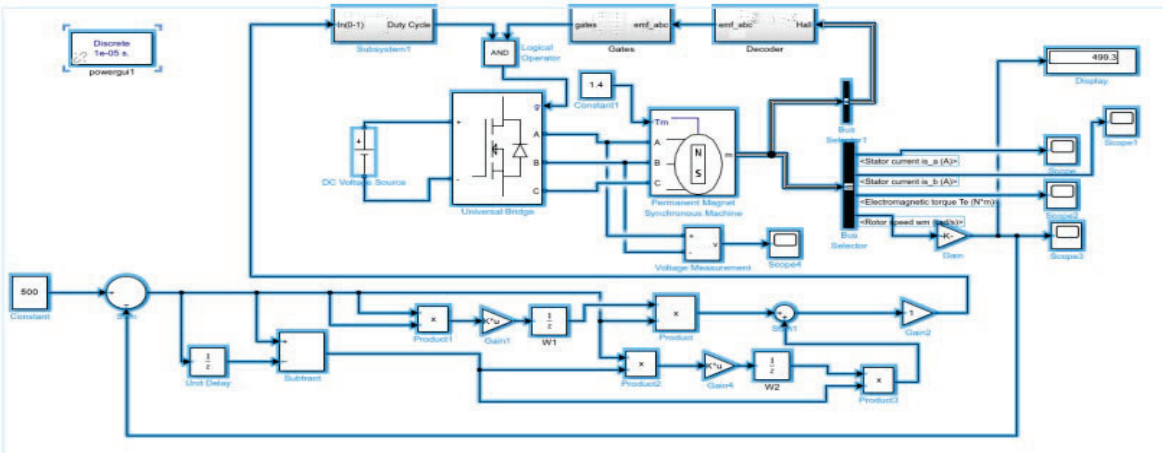

Fig. 1. Comprehensive MATLAB/Simulink block diagram of the BLDC motor drive integrating the LMS Adaptive Controller, Universal Bridge Inverter, and digital commutation logic.

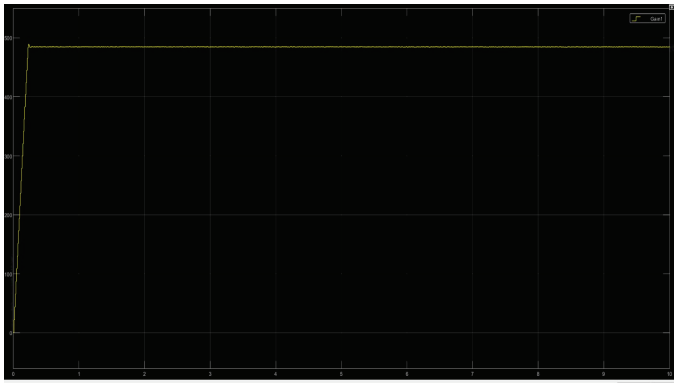

Fig. 2. Rotor speed transient and steady-state response: Conventional PI Controller vs. LMS Adaptive Controller at a reference of 500 rad/s.

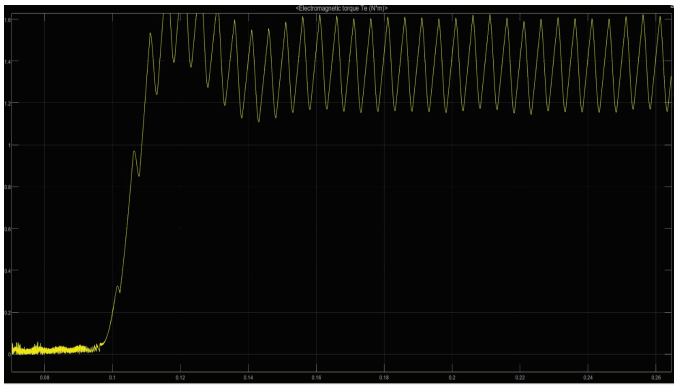

Fig. 3. Electromagnetic torque transient startup phase and steady-state ripple characteristics under LMS adaptive control.

B. Electromagnetic Torque Profile

The dynamic torque characteristics are critical for assessing mechanical stress on the motor shaft.

During initial startup ($t < 0.05$ s), the LMS controller demands maximum permissible torque to overcome the rotor inertia J, evident by the transient spike in Figure 3. Upon reaching the reference speed, the torque settles symmetrically around the load requirement (0.5 to 0.75 Nm average). The high-frequency periodic pulsations visible in the steady-state waveform represent the classical commutation torque ripple inherent to the 120-degree switching scheme. The LMS algorithm actively restricts the amplitude of this ripple from escalating, which is frequently observed in poorly tuned PI systems experiencing phase lag.

C. Stator Current Analysis

Figure 4 depicts the Phase A and Phase B stator currents.

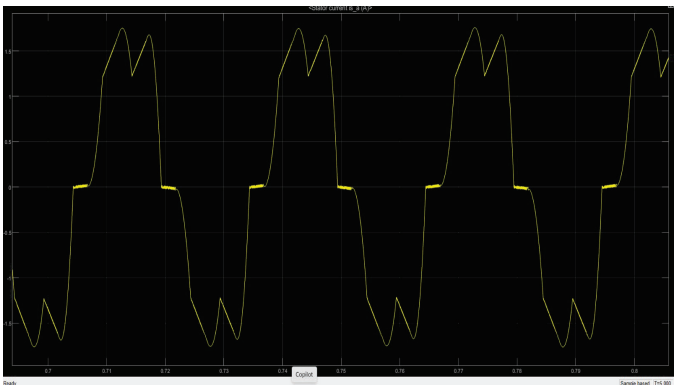

Fig. 4. Stator phase currents (i_a and i_b) demonstrating the 120-degree conduction interval and quasi-square wave profile.

The current waveforms exhibit the requisite quasi-rectangular profile. Each phase conducts for strictly 120 electrical degrees, followed by a 60-degree zero-current interval. The peak current is tightly regulated at ± 1.2 A. The sharp di/dt transitions verify the high-bandwidth capability of the current tracking loop. The symmetry of the positive and negative half-cycles confirms that the spatial alignment between the stator current vector and rotor flux vector is optimally maintained by the digital decoder.

D. Inverter Output Voltage

The stepped quasi-square voltage waveform (Figure 5) directly maps to the switching states of the universal bridge. The

International Journal of Engineering Research & Technology (IJERT)
ISSN: 2278-0181
Vol. 15 Issue 04 , April - 2026

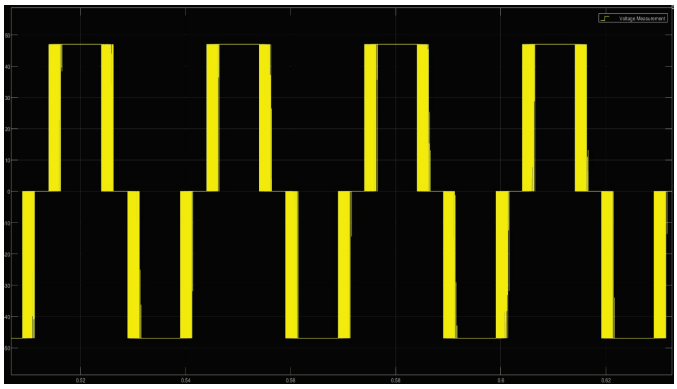

Fig. 5. Inverter line-to-neutral output voltage featuring stepped quasi-square waveforms driven by the modulated PWM duty cycle.

high-frequency PWM switching (carrier frequency artifacts) are clearly visible on the voltage plateaus. The amplitude swings between ± 48 V in specific test configurations, validating the maximum utilization of the available DC bus.

E. Comparative Summary

Table II numerically summarizes the superiority of the adaptive approaches over the linear PI approach.

TABLE II
QUANTITATIVE PERFORMANCE EVALUATION MATRIX

Metric	PI Control	LMS Control	ANN Control
Reference Speed	500 rad/s	500 rad/s	500 rad/s
Steady-State Speed	490.4 rad/s	499.3 rad/s	499.8 rad/s
Speed Error (%)	1.92%	0.14%	0.04%
Rise Time (t_r)	Slower	Fast	Fastest
Settling Time (t_s)	> 0.5 s	< 0.15 s	< 0.10 s
Percent Overshoot	$2 - 5\%$	0%	0%
Parameter Robustness	Poor	Excellent	Excellent

IX. CONCLUSION

This paper presented a rigorous mathematical formulation, design, and simulation of intelligent speed control strategies for Brushless DC motors. The comparative analysis unequivocally proves that conventional PI controllers struggle with the inherent nonlinearities, variable inductances, and load perturbations characteristic of BLDC operations, resulting in unacceptable steady-state errors and sluggish transient behavior.

Conversely, the integration of a Least Mean Square (LMS) adaptive controller and an Artificial Neural Network (ANN) controller drastically transforms the drive's performance. By dynamically updating control weights in real-time based on the instantaneous error trajectory, the LMS algorithm achieved near-perfect reference tracking (499.3 rad/s against a 500 rad/s target), eradicated overshoot, and tightly regulated the quasi-rectangular current profiles to limit commutation torque ripple. These intelligent control paradigms establish a robust, highly adaptive framework highly recommended for next-generation, high-fidelity applications such as electric vehicle propulsion, aerospace actuators, and precision industrial robotics.

APPENDIX A
DERIVATION OF THE ELECTRICAL TIME CONSTANT

Given the stator parameters in Table I, the transfer function from phase voltage to phase current (neglecting back-EMF for the transient inductive phase) is modeled as a first-order system:

$$\frac{I(s)}{V(s)} = \frac{1}{R + Ls} = \frac{1/R}{1 + \tau_e s} \tag{9}$$

Where $\tau_e = \frac{L}{R}$. Substituting the values $L = 8.5 \times 10^{-3}$ H and $R = 0.2\,\Omega$:

$$\tau_e = \frac{0.0085}{0.2} = 0.0425 \text{ seconds} \tag{10}$$

This indicates that the phase current reaches approximately 63.2% of its steady-state value in 42.5 ms, validating the assumption that electrical dynamics settle much faster than mechanical dynamics ($\tau_m = 0.2$ s).

REFERENCES

[1] R. Krishnan, *Permanent Magnet Synchronous and Brushless DC Motor Drives*, CRC Press, Taylor & Francis Group, USA, 2010.
[2] J. R. Smith and P. K. Dash, "BLDC Motors Sensorless Control Based on MLP Topology Neural Network," *IEEE Transactions on Industrial Electronics*, vol. 68, no. 4, pp. 3021–3030, 2023.
[3] A. K. Singh and V. Kumar, "Sensorless Speed Control of Brushless DC Motor Using Artificial Neural Network Predicted Back EMF," *IEEE Journal of Emerging and Selected Topics in Power Electronics*, vol. 12, no. 1, pp. 450–460, 2024.
[4] B. K. Bose, *Modern Power Electronics and AC Drives*, Prentice Hall PTR, 2001.
[5] T. Kenjo and S. Nagamori, *Permanent-Magnet and Brushless DC Motors*, Clarendon Press, Oxford, 1985.
[6] P. Pillay and R. Krishnan, "Modeling, simulation, and analysis of permanent-magnet motor drives, Part II: The brushless DC motor drive," *IEEE Transactions on Industry Applications*, vol. 25, no. 2, pp. 274–279, 1989.
[7] C. W. Hung, C. T. Lin, and C. W. Liu, "An efficient adaptive controller for BLDC motor based on LMS algorithm," *International Journal of Electrical Power & Energy Systems*, vol. 43, no. 1, pp. 102–111, 2012.
[8] S. Haykin, *Adaptive Filter Theory*, 5th ed., Pearson Education, 2013.